Spectral properties and crystal-field splittings in CeM_2Si$_2$ (M=Ru, Rh, or Pd) compounds

V. Vildosola and A. M. Llois
Departamento de Física, Comisión Nacional de Energía Atómica, Av. Gral. Paz 1499 - (1650) San Martín, Argentina and Departamento de Física, J. J. Giambiagi, FCEyN, Universidad de Buenos Aires, Buenos Aires, Argentina

M. Alouani
IPCMS-GEMME, UMR 7504 CNRS-ULP, 23 rue du Loess, F-67034 Strasbourg Cedex, France
(Received 17 December 2004; revised manuscript received 28 February 2005; published 27 May 2005)

The crystal-field splittings and the spectral properties of the CeM_2Si$_2$ compounds (M=Ru, Rh, and Pd) are studied by means of an *ab initio* many-body combined technique. The hybridization function is obtained using the local-density approximation and the full-potential linear augmented plane wave method and is used as input to the Anderson impurity model. The Kondo physics is obtained by solving this model within an extended noncrossing approximation. The calculated crystal electric-field (CEF) splittings are compared with the contradictory experimental data and helped in the correct assignment of their symmetries. In particular, it is shown that the CeRh$_2$Si$_2$ has the largest CEF splittings and the highest Kondo temperature, in good agreement with experimental data. The position of the bare energy f level is found to affect slightly the CEF splittings but does not change their symmetries.

DOI: 10.1103/PhysRevB.71.184420 PACS number(s): 71.27.+a, 71.70.Ch, 71.20.Eh

I. INTRODUCTION

The unusual and interesting physical properties of rare-earth intermetallic compounds have their origin in the combination of strongly correlated $4f$ states and the hybridization with the conduction electron sea, which give rise to their complex low-temperature Kondo behavior. In particular, Ce compounds are very sensitive to the crystalline and chemical environment as compared to other rare-earth systems. The interaction of the $4f$ state with the conduction band plays an important role in the determination of the different magnetic, structural, and transport properties of these systems.

Strongly correlated Ce compounds require a many-body formalism to describe the dynamical effects. However, in the most usual many-body treatments, the details of the chemical bonding, provided by the band structure, are not usually taken into account. It has become a challenge for theoreticians to accomplish implementations of realistic models combining both aspects of the physical properties of these systems, namely, the electronic structure characteristics and the many-body correlation effects.[1–4]

In this respect, the family CeM_2Si$_2$ is a good example of materials for which the detailed knowledge of the electronic structure of the conduction band is required when studying their physical properties. Depending on the hybridization strength of the $4f$ electrons, this class of materials exhibits a wide variety of low-temperature behaviors such as long-range magnetic order, heavy fermion character, paramagnetism, nonmagnetic order with magnetic correlations, and superconductivity, among others.[5]

In this work, we focus our attention on CeRu$_2$Si$_2$, CeRh$_2$Si$_2$, and CePd$_2$Si$_2$, where Ru, Rh, or Pd are adjacent to each other in the Periodic Table. Although the three compounds crystallize in the same tetragonal ThCr$_2$Si$_2$ structure, the electronic properties are considerably different. These properties can be briefly summarized as follows. The CeRu$_2$Si$_2$ compound is a heavy fermion, and its low-temperature behavior is well described by a paramagnetic Fermi liquid, in which no long-range magnetic order has been observed down to 20 mK. The low-energy excitations are strongly renormalized heavy quasiparticles, as inferred from the large value of its specific-heat coefficient γ.[6,7] On the other hand, CePd$_2$Si$_2$ and CeRh$_2$Si$_2$ show antiferromagnetic ordering (AF) with Néel temperatures, respectively, of $T_N \sim 10$ K and 36 K. Both systems show a rather fast decrease in the value of T_N with applied pressure, which is the prelude of pressure-induced superconductivity. In CePd$_2$Si$_2$, the critical hydrostatic pressure at which AF is suppressed is $P_C \sim 2.5$ GPa, while for CeRh$_2$Si$_2$ it is much lower, $P_C \sim 0.9$ GPa.[8–10]

The large ordering temperature of CeRh$_2$Si$_2$ and an almost free-ion magnetic moment on the Ce site ($\mu_{ord} = 1.5\mu_B$) (Ref. 11) suggest that the $4f$ states are quite localized in this compound. On the other hand, the evolution of these quantities with applied hydrostatic pressure and the large value of the Kondo temperature ($T_K \approx T_N$), as compared to other compounds of the CeM_2Si$_2$ family, lead to the assumption that the $4f$ states are strongly hybridized and quite delocalized.[12] Another peculiar feature of CeRh$_2$Si$_2$, making it a singular system in this class of materials, is its highest value of the c/a ratio of its lattice parameters.

In a previous work, we studied the influence of the $4f$ hybridization on the structural and electronic properties of these tetragonal compounds and their evolution with applied pressure.[13] In particular, the calculated evolution of Ce-M distances and spin magnetic moment with pressure indicates that the strength of $4f$-$4d$ hybridization in the CeM_2Si$_2$ series increases with decreasing $4d$ band filling, i.e., the CeRu$_2$Si$_2$ compound is most affected by the $4f$ hybridization and applied pressure. On the other hand, the evolution of the calculated c/a ratios with pressure shows considerable differences among the three systems. In contrast with the behavior of CeRu$_2$Si$_2$ and CePd$_2$Si$_2$, the c/a ratio of CeRh$_2$Si$_2$ is not

sensitive to the presence of $4f$ states in the valence band, indicating the anisotropy of the interactions in this particular compound. In spite of the localized nature of the $4f$ states in these systems, these results reveal the need to take into account the crystalline and chemical environment to understand correctly their electronic properties.

In this work, we employ a scheme that takes into account the realistic *ab initio* band structure of the material as well as the underlying strong correlation effects. This method permits the computation of both the hybridization-induced crystalline electric field splittings (CEF) and the spectral properties.

The knowledge of the CEF splittings of the $4f$ states is essential for the correct analysis and interpretation of thermal, transport, and spectral properties of these systems. Usually, after solving the crystal-field Hamiltonian of the Ce ion, these splittings are determined by fitting parameters to the experimental curves such as neutron scattering, specific heat, and magnetic susceptibility.[14,15] Unfortunately, there are discrepancies among the CEF splittings obtained through experimental fittings, even within the same experimental technique. These contradictions, which will be discussed later, reflect some difficulties in determining the correct ground state, and our results can help in the proper assignment of the symmetry of the CEF energy levels.

On the other hand, photoemission spectroscopy is a useful tool for investigating the $4f$ states and the mechanism of hybridization with the other bands in the solid. We expect to complement the study of these systems by calculating their spectral properties.

The *ab initio* many-body technique[1] consists, first, in calculating the hybridization function using the all-electron full-potential linearized augmented plane wave (FP-LAPW) method, and secondly, in using these hybridization functions as an input for the Anderson impurity model. The Kondo physics is then studied by solving this model within an extended *noncrossing approximation* similar to that performed by Han *et al.*[1]

II. METHOD OF CALCULATION

As mentioned above, we use the information coming from electronic band-structure calculations to parametrize a strongly correlated many-body Hamiltonian. In Ref. 1, this mixed technique was applied to Ce-based cubic systems calculating the hybridization function using the linearized muffin-tin orbital (LMTO) method in the atomic sphere approximation (ASA) within the local-density approximation (LDA). The hybridization function, $\Gamma(\varepsilon)$, was inserted in the Anderson impurity model, which, in turn, was solved in the $U\rightarrow\infty$ limit using an extended *noncrossing* approximation (NCA). We call this technique LDA-NCA from now on.

Within this impurity model, the interaction among different Ce sites is neglected and lattice effects such as long-range magnetic order or superconductivity are not taken into account.

In this work, we implement the LDA-NCA approach for the tetragonal compounds, and calculate the $\Gamma(\epsilon)$ functions from a full-potential linearized augmented plane wave method (FP-LAPW).[16] Thus, we improve upon Ref. 1 by avoiding any further approximations concerning the shape and the form of the potential.

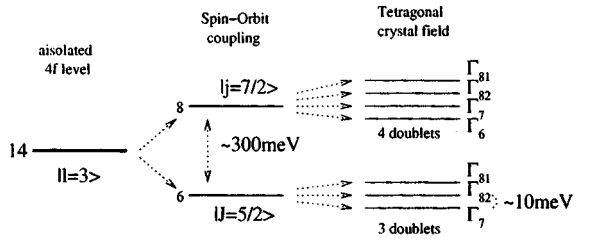

$J=\frac{5}{2}$	$J=\frac{7}{2}$
$\Gamma_7 = a\left\|\frac{5}{2};\pm\frac{5}{2}\right\rangle - b\left\|\frac{5}{2};\mp\frac{3}{2}\right\rangle$	$\Gamma_6 = c\left\|\frac{7}{2};\pm\frac{7}{2}\right\rangle + d\left\|\frac{7}{2};\mp\frac{1}{2}\right\rangle$
$\Gamma_{82} = b\left\|\frac{5}{2};\pm\frac{5}{2}\right\rangle + a\left\|\frac{5}{2};\mp\frac{3}{2}\right\rangle$	$\Gamma_7 = e\left\|\frac{7}{2};\pm\frac{5}{2}\right\rangle - f\left\|\frac{7}{2};\mp\frac{3}{2}\right\rangle$
$\Gamma_{81} = \left\|\frac{5}{2};\pm\frac{1}{2}\right\rangle$	$\Gamma_{82} = d\left\|\frac{7}{2};\pm\frac{7}{2}\right\rangle - c\left\|\frac{7}{2};\mp\frac{1}{2}\right\rangle$
	$\Gamma_{81} = f\left\|\frac{7}{2};\pm\frac{5}{2}\right\rangle + e\left\|\frac{7}{2};\mp\frac{3}{2}\right\rangle$

FIG. 1. Irreducible representations of the tetragonal point group symmetry at the Ce site for the CeM_2Si_2 compounds. The values used for the different parameters were taken from Ref. 18. They are $a=\sqrt{\frac{1}{6}}$, $b=\sqrt{\frac{5}{6}}$, $c=\sqrt{\frac{5}{12}}$, $d=\sqrt{\frac{7}{12}}$, $e=\sqrt{\frac{3}{4}}$, and $f=\frac{1}{2}$.

For Ce systems, the Anderson impurity Hamiltonian has the form

$$H=\sum_{k\sigma}\varepsilon_k c^\dagger_{k\sigma}c_{k\sigma}+\sum_m \varepsilon_{fm}f^\dagger_m f_m + U\sum_{m>m'} n_{fm}n_{fm'} + \sum_{k\sigma,m}(V_{k\sigma,m}f^\dagger_m c_{k\sigma}+\text{H.c.}), \quad (1)$$

where $V_{k\sigma,m}$ is the hopping matrix element between the conduction electrons ($c_{k\sigma}$) and the $4f$ orbital (f_m), ε_{fm} is the $4f$-energy level with respect to the Fermi level, and U is the on-site Coulomb repulsion of the $4f$ electrons. The Γ function is proportional to $V^*_{k\sigma,m}V_{k\sigma,m}$ and, as suggested by Gunnarsson *et al.*,[17] it can be estimated from the projected LDA $4f$ density of states ρ^{LDA}_m at the Ce site in the following way:

$$\Gamma_m(\varepsilon) = -\,\text{Im}\left\{\lim_{\eta\rightarrow 0}\left[\left(\int dz\frac{\rho^{\text{LDA}}_m(z)}{\varepsilon - i\eta - z}\right)\right]^{-1}\right\}. \quad (2)$$

In the case of the CeM_2Si_2 compounds, the label m corresponds to the different irreducible representations of the $4f$ states at the tetragonal Ce site. In the tetragonal point group, the $J=\frac{5}{2}$ and $J=\frac{7}{2}$ multiplets are split into three and four doublets, respectively, as shown in Fig. 1.

The $U\rightarrow\infty$ limit of the Anderson impurity model is solved by applying the slave-boson technique. The NCA equations consist of a couple of integral nonlinear equations for the pseudoboson (f^0) and pseudofermion (f^1) self-energies, each of them containing the hybridization function $\Gamma(\epsilon)$. For a detailed review of the NCA formalism, see Refs. 19,20.

Within this approach, the value of the *bare* $4f$ level, ε_f, is a quasifree parameter kept close to its atomic limit. We do

calculations for different values of ε_f in the energy range of $(-1.6\ \text{eV}, -3.0\ \text{eV})$. One of course could obtain the value of the $4f$ level by means of a constrained LDA method in conjunction with the so-called supercell technique as done by Cooper and co-workers for the CeSb and CeTe compounds.[2] Unfortunately, such calculations are time-consuming and beyond our computational facilities. In addition, it is not clear whether the position of the $4f$ level obtained this way will be appropriate for the Anderson model within the NCA, where the Coulomb interaction is set to infinity. A $4f$ level obtained this way might be more appropriate for the Gunnarsson and Schönhammer approach[21] or the treatment of the Anderson model by means of the dynamical mean-field theory (DMFT),[22] where the Coulomb interaction is finite and could also be obtained from the same constrained LDA. As for the spin-orbit (SO) splitting between the $J=\frac{5}{2}$ and $J=\frac{7}{2}$ multiplets (Δ_{SO}), we took its value from the $4f$-projected DOS as in Ref. 1. For the systems under study, our calculation shows $\Delta_{\text{SO}}=0.31\pm0.01$ meV, which is in agreement with the observed SO peaks in photoemission spectra.[23–25]

We perform the *ab initio* band-structure calculations for the CeM_2Si_2 compounds using the experimental lattice parameters. We use the LDA exchange and correlation potential of Perdew and Wang.[26] To sample the Brillouin zone and converge the total energy up to 0.1 meV accuracy, we used a mesh of 1000 $\boldsymbol{k}$ points (99 irreducible $\boldsymbol{k}$ points). The *muffin-tin* radii, R_{mt}, are taken equal to 2.6 a.u. for Ce, 2.2 a.u. for the $4d$ transition metals, and 2.0 a.u. for Si. The cutoff parameter that gives the number of plane waves in the interstitial region was taken as $R_{\text{mt}}K_{\text{max}}=8$, where K_{max} is the largest reciprocal-lattice vector used in the expansion of plane waves in that region. This cutoff implies 120 plane waves per atom approximately.

III. RESULTS

Figure 2 shows the hybridization function $\Gamma(\varepsilon)$ calculated for the three compounds under study. For simplicity, we only plot the hybridization for the Γ_7 doublet, which will be shown later to be the symmetry of the ground state. It can be seen that the main weight of the hybridization function is shifted towards higher energies when M goes from Pd to Ru. These results can be understood if we take into account that the main contribution to the hybridization of the $4f$ states in these compounds originates from the $4d$ band of the transition metal M. The calculated $4d$ band centers are indicated with arrows in Fig. 2, and it can be observed that they are shifted towards higher energies with decreasing $4d$ occupation numbers. These results explain also the higher sensitivity of the Ru compound when applying hydrostatic pressure as compared to the systems with Rh or Pd, as discussed in a previous work.[13]

In the following we present the results obtained with the LDA-NCA technique: in Sec. III A, we present the CEF splittings, and in Sec. III B, we present the spectral properties.

A. CEF splittings

The LDA-NCA technique permits the computation of the CEF splittings and the symmetry of each $4f$ level. The splittings are read from the separation of the peaks of the different spectral functions, ρ_m's, which are shifted one with respect to the other due to a different degree of hybridization of each $4f$ level with the conduction band.

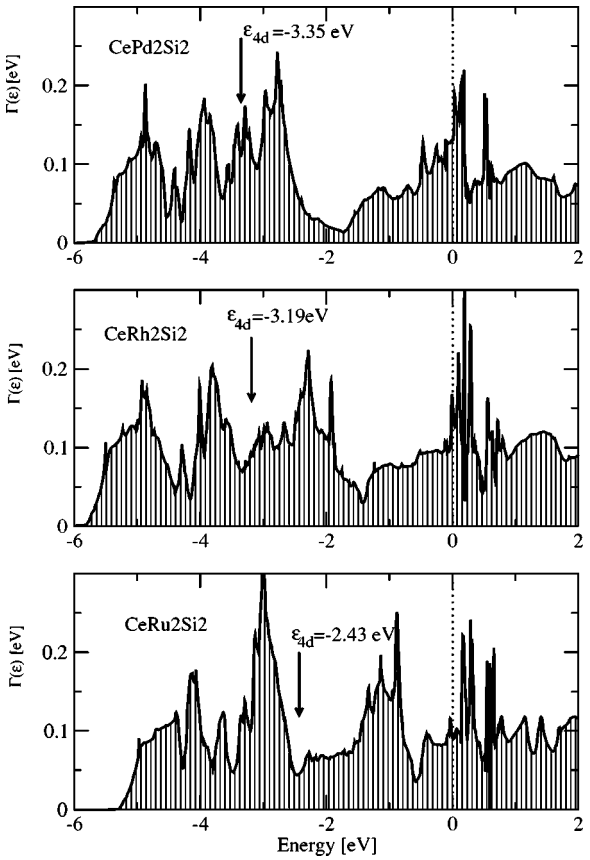

FIG. 2. Hybridization function $\Gamma(\varepsilon)$ for CeM_2Si_2 with M=Ru, Rh, or Pd for the Γ_7 symmetry. The dotted line indicates the Fermi level in each system. The arrows correspond to the $4d$ band center of the transition metal M.

In Table I, the compiled experimental information taken from the literature for these quantities is shown. We call Δ_{12} the energy difference between the lowest energy level and the first excited one and Δ_{23} the corresponding energy difference between the first and second excited levels of the $J=\frac{5}{2}$ multiplet.

In the case of $CeRu_2Si_2$, there is no clear information on the second excited state. For this particular system, we also include plausible values for CEF splittings considered in other theoretical calculations. From Table I, it is evident that the information found in the literature is contradictory, especially the one related to the determination of the symmetries. This makes it difficult to compare these values with our results.

As mentioned above, within this LDA-NCA technique the bare $4f$ level ε_f is a quasifree parameter. We perform the calculations varying ε_f within the range $(-3\ \text{eV}, -1.6\ \text{eV})$. In Fig. 3, we present the LDA-NCA results (left) together with some experimental information (right). The results appearing in Fig. 3 were obtained using the value for ε_f which better fits the experimental data for each compound. These values are $\varepsilon_f=-1.6$ eV for $CeRu_2Si_2$ and $CeRh_2Si_2$

TABLE I. Compilation of literature information about CEF splittings (Δ_{12} and Δ_{23}), and symmetry of $J=\frac{5}{2}4f$ levels. In the last column, χ refers to magnetic susceptibility measurements. In the case of $CeRu_2Si_2$, the question mark in the first row indicates that the second excited CEF level was not found. (*) In Ref. 15, the neutron-scattering spectra suggest the existence of CEF excited states in the energy range indicated in the table. (**) Parameters used for CEF splittings in an NCA calculation to fit photoemission spectra (see Ref. 24). (***) CEF splittings suggest in Ref. 31 to perform renormalized band calculation.

Compound	Δ_{12}, Δ_{23}	symmetry	Reference
$CePd_2Si_2$	220 K,20 K	$\Gamma_{82}-\Gamma_7-\Gamma_{81}$	Neutron scatt.[15]
	260 K,30 K	$\Gamma_{82}-\Gamma_7-\Gamma_{81}$	χ[27]
	220 K,60 K	$\Gamma_7-\Gamma_{81}-\Gamma_{82}$	χ[28]
$CeRh_2Si_2$	310 K,370 K	$\Gamma_7-\Gamma_{82}-\Gamma_{81}$	χ[29]
	370 K,560 K	$\Gamma_{82}-\Gamma_{81}-\Gamma_7$	χ[27]
$CeRu_2Si_2$	220 K,?	-	Specific heat[30]
	$\Delta_{12}+\Delta_{23_i}$ 400 K	-	(*)
	150 K,150 K	-	(**)
	220 K,180 K	$\Gamma_7-\Gamma_{81}-\Gamma_{82}$	(***)

and $\varepsilon_f=-2.4$ eV for $CePd_2Si_2$. To facilitate the comparison, not all the data presented in Table I appear in Fig. 3.

Three main points that emerge from the comparison with experiments can be singled out from the analysis of Fig. 3. First, it can be seen that both our results and the experiments indicate that $CeRh_2Si_2$ has the greatest total CEF splitting ($\Delta_{12}+\Delta_{23}$) among the three systems. Second, there is also agreement concerning the almost degenerate first and second excited levels in $CePd_2Si_2$. Finally, our results determine that the symmetries of the lowest, first, and second excited levels are Γ_7, Γ_{82}, and Γ_{81}, respectively.

It is crucial to notice that the calculated symmetries for each level do not change with ε_f, along the whole range of variation of this parameter. The experimental results of Ref. 29 in the case of $CeRh_2Si_2$ agree completely with this ordering for the symmetry of the levels. Actually, we cannot go

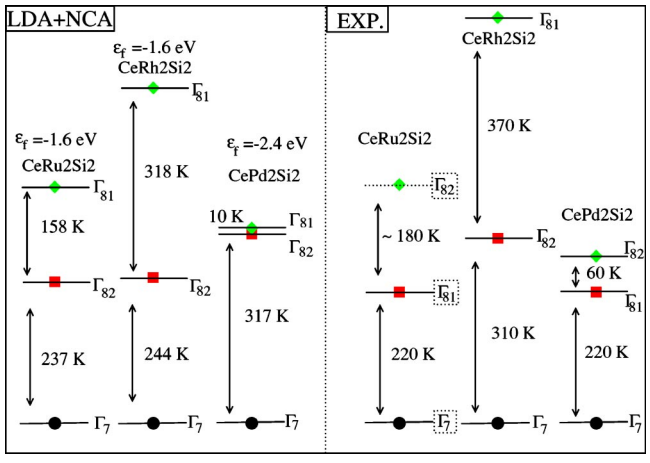

FIG. 3. Crystal-field splittings of the $4f$ states $\left(J=\frac{5}{2}\right)$. To the left: The results using ε_f as input parameter equal to -1.6 eV for $CeRu_2Si_2$ and $CeRh_2Si_2$, and -2.4 eV for $CePd_2Si_2$. To the right: selected experimental data taken from Table I. The corresponding symmetry of each level is indicated on the right side. There is no precise experimental information about the second excited state of the $CeRu_2Si_2$, which is why it appears as a dotted line.

further in the comparison of the symmetries due to the contradictions among the different experimental results.

The first two points mentioned above are related to the value of the splittings. The fact that $CeRh_2Si_2$ has the largest total splitting reflects the anisotropy of this system, which is a consequence of its large c/a ratio. Namely, c/a is 2.49 in the system with Rh while it is 2.33 in the cases of Ru or Pd.[13] As shown in Ref. 13, this anisotropy affects the evolution of the structural properties under pressure and, as we see in the present work, it also affects the CEF splittings.

Even if the overall agreement with the experimental trends is already present in our results, there are actually some differences. For instance, the calculated value of Δ_{12} for $CePd_2Si_2$ is greater than any other in the series, while this is not the case in the experiments. On the other hand, for $CeRh_2Si_2$, both Δ_{12} and Δ_{23} are smaller than the experimental splittings. One of the reasons for these discrepancies is probably because the NCA neglects the double occupancy of the $4f$ state.

While the symmetries of each level do not change when shifting ε_f, the values of the splittings Δ_{12} and Δ_{23} are sensitive to this parameter. As already mentioned, the results shown in Fig. 3 were obtained considering $\varepsilon_f=-1.6$ eV for the system with Ru or Pd, and $\varepsilon_f=-2.4$ eV for $CePd_2Si_2$. Even though this choice of parameters gives trends for the CEF splittings in quite good agreement with the experimental data, a value of ε_f close to -2 eV is expected for these strongly correlated Ce compounds.

Figure 4 presents the calculated CEF splittings considering $\varepsilon_f=-2$ eV for the systems with Ru and Rh, and keeping $\varepsilon_f=-2.4$ eV for $CePd_2Si_2$ (left) together with the same selected experimental information of Fig. 3 (right). It can be seen that shifting ε_f to more negative energies in these two compounds has the effect of reducing the splittings. In spite of this, the results discussed above are still valid for this new set of parameters. The $CeRh_2Si_2$ has still the largest total CEF splitting ($\Delta_{12}+\Delta_{23}$), the first and second excited states in $CePd_2Si_2$ are almost degenerate, and the orderings of the symmetries for the lowest, first, and second excited levels are Γ_7, Γ_{82}, and Γ_{81}, respectively. This new set of parameters

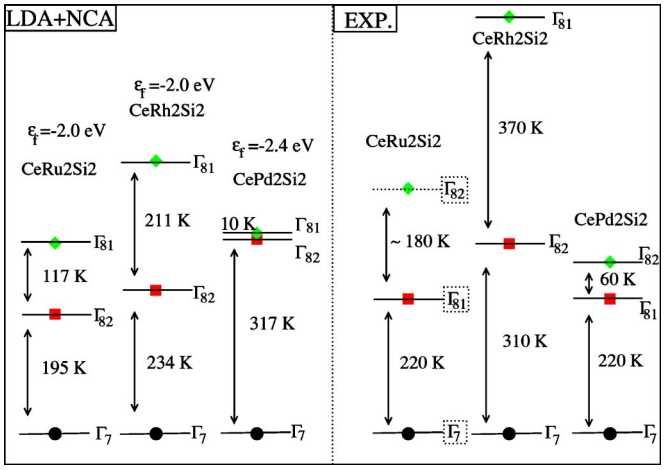

FIG. 4. Crystal-field splittings of the $4f$ states $\left(J=\frac{5}{2}\right)$. To the left: The results using ε_f equal to −2 eV for $CeRu_2Si_2$ and $CeRh_2Si_2$ and −2.4 eV for $CePd_2Si_2$. To the right: The same literature information compiled in Fig. 3. The corresponding symmetry of each level is indicated on the right side.

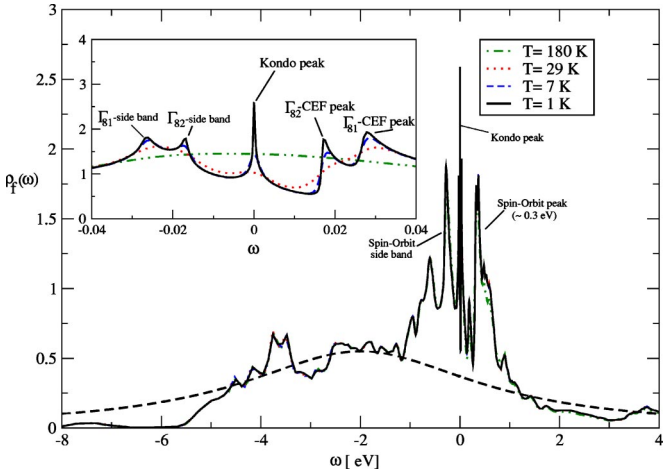

FIG. 5. Spectral function calculated for $CeRu_2Si_2$ at four different temperatures. The ionization $4f$ peak is centered around $-\varepsilon_f$ over which the electronic band structure is mounted. The dashed curve is a Lorentzian centered at $-\varepsilon_f$ to facilitate the identification of this peak. Close to the Fermi level (E_F), the Kondo peak can be observed (screening of the localized electron in the Γ_7 level). The CEF and the SO peaks appear around 20 and 300 meV, respectively, above E_F, accompanied by the corresponding side bands at negative energies. In the inset, we show the low-energy peaks.

gives rise to more realistic spectral properties, as will be shown in the following section. Nevertheless, one should not rule out that a finite value of the Coulomb interaction will alter the symmetry of the ground state of these compounds. A point-charge model, as done by Birgenau *et al.*[32] for cerium monopnictides, will certainly help in the interpretation of the present results. Unfortunately, no such calculations are performed for the present experimental CEF of these compounds.

B. Spectral properties

The spectral function given by $\rho_f(\omega)=-(1/\pi)\mathrm{Im}[G_f(\omega+i0^+)]$, where G_f is the $4f$ Green function obtained by solving the NCA equations of the Hamiltonian of Eq. (1), was calculated using the same set of parameters as for the CEF's of Fig. 4.

In Fig. 5, we show the calculated spectral function for $CeRu_2Si_2$ at four different temperatures. The sensitivity to temperature is only noticeable at low energies (see the inset of Fig. 5). The fine structure along the whole energy range comes from the dependence on energy of the hybridization function. Several features in the spectral function of Fig. 5 are disguised by the band structure. There is a peak centered around $-\varepsilon_f$ that accounts for the occupied $4f$-Γ_7 level, which we call the ε_f peak. In order to identify this peak, a Lorentzian is superimposed (dashed line). The antiferromagnetic screening of this localized level provided by the conduction band gives rise to the Kondo resonance close to the Fermi level (0 eV). Since the probability for the occupation of the excited levels is small but not null, excitation peaks appear at negative energies (side bands) corresponding to two different energy scales: SO scale ($-\Delta_{SO}\sim-0.3$ eV) and CEF scale ($-\Delta_{CEF}\sim-10$ meV). This last set of peaks is depicted in the inset of Fig. 5, and it can be observed how they are turned on as temperature goes down. Consequently, if there is a nonzero probability of occupying excited levels, there is a nonzero probability for these excited levels to be antiferromagnetically screened by the conduction band, giving rise then to Kondo-like peaks at the corresponding positive energies, which lie around $\Delta_{CEF}+T_K$, in the case of the CEF excitations, and around $\Delta_{SO}+T_K$ for the spin-orbit ones. See Ref. 20 for a detailed interpretation of the different peaks appearing in ρ_f applied to a simpler model which considers a flat density of states for the conduction band.

In Fig. 6, we plot $\rho_f(\omega)$ in the range -6 eV$<\omega<0$ eV in order to compare the shape of the ε_f peak and the relative intensity to the SO peak in the three compounds. In the case of $CePd_2Si_2$, the spectral function (solid line in Fig. 6) presents well defined ε_f and SO peaks (this last one indicated with an arrow). The intensity of the first peak is considerably

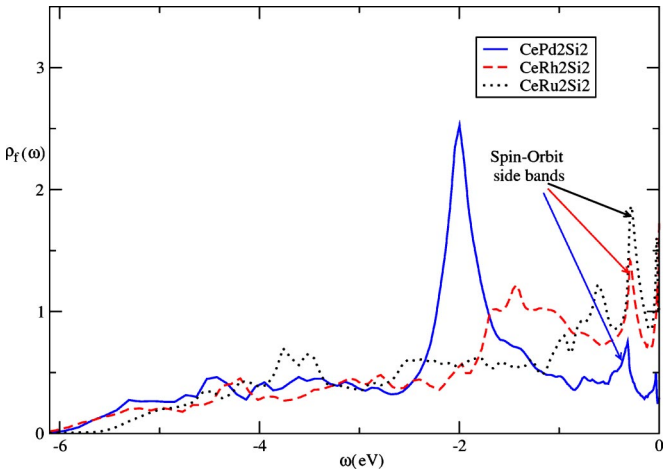

FIG. 6. Calculated spectral function for CeM_2Si_2 (M=Ru, Rh, or Pd).

larger than that of the second one. On the other hand, the ε_f peak in $CeRh_2Si_2$ (dashed line, same figure) is less defined than in the system with Pd, as it is wider and more influenced by the band structure. In contrast to what happens in the case with Pd, the intensity of the ε_f and SO peaks is of the same order. Finally, in the case of $CeRu_2Si_2$ (dotted line), the ε_f peak in the spectral function is disfigured by the band structure and it can be assured that the intensity of the SO peak is higher than any other peak in the spectra. These features are also noticeable in the experimental curves (see Ref. 23 for $CeRu_2Si_2$ and $CeRh_2Si_2$ and Ref. 25 for $CePd_2Si_2$). That is, the ε_f peak is better defined in the system with Pd than in the other two systems and its intensity is larger than that of the SO peak. The intensity difference between these two peaks decreases in the compounds $CeRh_2Si_2$ and $CeRu_2Si_2$. In particular, the calculated ρ_f and the experimental spectrum in the system with Ru agree in the sense that the SO peak is higher than the ε_f peak.

The shape evolution of the ε_f peak along the three compounds can be understood in terms of the transition-metal *4d* band filling. The more occupied the *4d* band is, the weaker is the *4f-4d* hybridization and the less influenced is the corresponding ε_f peak by the electronic structure in the spectral function.

With respect to the low-energy peaks mentioned above, in the inset of Fig. 5, it can be observed how the Kondo peak turns on as the temperature goes down, which means that the singlet state accounting for the antiferromagnetic coupling of the localized *4f* electron with the conduction band is being formed. Although this Kondo state starts to develop in the three systems under study, it was not possible to achieve low enough temperatures in order to complete the formation of this state due to numerical instabilities and, consequently, a reliable estimation of the Kondo temperatures is lacking. However, we can infer the trends in T_K's for these compounds. Experimentally, it is known that the Kondo temperatures are around 20 K for $CeRu_2Si_2$,[24] 35 K for $CeRh_2Si_2$,[29] and 10 K for $CePd_2Si_2$.[28] In Fig. 7, we plot the calculated *4f* spectral function (solid curve) in the range where the CEF's are important, for the three systems and at a temperature sufficiently low so that the Kondo peak can be clearly observed. It can be seen that the Kondo peak in the system with Rh is more developed than in the system with Ru and subsequently more than in the system with Pd. This result indicates that if the Kondo regime would be completely attained, $CeRh_2Si_2$ would reach it at higher temperatures than $CeRu_2Si_2$, and $CeRu_2Si_2$ at a higher T_K than $CePd_2Si_2$. From this, we can expect from our results that $T_K(CeRh_2Si_2) > T_K(CeRu_2Si_2) > T_K(CePd_2Si_2)$, in agreement with the experimental trends for the T_K's.

In Fig. 7, we plot the $J=\frac{5}{2}$ components of the total spectral function ρ_f, ρ_7 (dashed line), ρ_{82} (dotted line), and ρ_{81} (dashed-dotted line) together with the total ρ_f (solid line). From this decomposition we can trace again the same characteristics of the crystal-field splittings obtained in Sec. III A. Namely, ρ_{82} and ρ_{81} are nearly degenerate in $CePd_2Si_2$, $CeRh_2Si_2$ presents the greater splitting among the three systems, and the lowest *4f* level has Γ_7 symmetry in all cases.

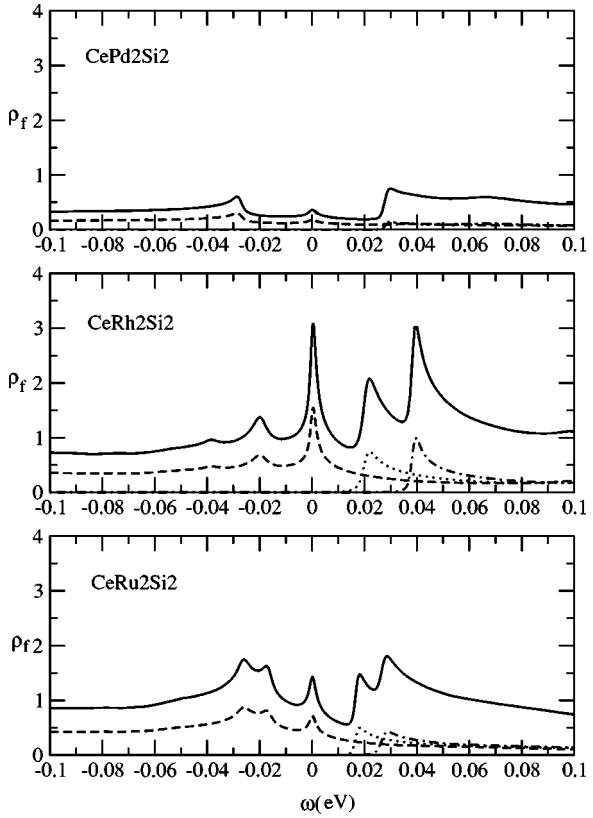

FIG. 7. Solid curve: total *4f* spectral function for CeM_2Si_2 (M = Ru, Rh, or Pd) in the CEF scale calculated at 7 K. The dashed curve is the Γ_7 component of the spectral function and the dotted and dashed-dot curves correspond to the Γ_{82} and Γ_{81} components, respectively.

IV. DISCUSSION AND CONCLUSIONS

In this paper, we apply a combined *ab initio* many-body technique to the CeM_2Si_2 (M = Ru, Rh, or Pd) materials. This technique contemplates two important aspects in Ce systems: The electronic structure which carries the information of the chemical bonding and crystalline environment of the Ce site and the many-body effects which give rise to the low-energy physics such as the Kondo effect.

This technique allowed us to calculate the crystal-field splittings of the *4f* states and to establish their symmetry. Our results indicated that the symmetries of the ground, first, and second excited states are Γ_7, Γ_{82}, and Γ_{81}, respectively, for the three compounds (see Fig. 1 for the notation). These results are independent of the choice of the position of the bare f level, ε_f, which is the only quasifree parameter used within this technique. It is difficult to make a comparison of our results with experimental data due to the existing contradictions in the literature, especially in the determination of the symmetries (see Table I).

With respect to the value of the splittings, we can point out two features which completely agree with the experimental available information: $CeRh_2Si_2$ presents the largest total splitting among the three compounds, and the first and second excited levels in $CePd_2Si_2$ are nearly degenerate. We observe that the absolute value of the splittings depends on ε_f. The experimental splittings are better reproduced if we

set $\varepsilon_f=-1.6$ eV for $CeRu_2Si_2$ and $CeRh_2Si_2$ and $\varepsilon_f=-2.4$ eV for $CePd_2Si_2$. However, the value −1.6 eV for the systems with Rh and Ru is not quite consistent with the photoemission spectra. We consider, therefore, the results obtained using $\varepsilon_f=-2$ eV for $CeRu_2Si_2$ and $CeRh_2Si_2$ to be more realistic. One of the reasons for the discrepancies between our calculations and the experiments, with respect to the value of the splittings, is that this method neglects the double occupancy of the $4f$ state ($U\rightarrow\infty$).

We also apply the LDA-NCA technique to study the spectral properties of these compounds. We obtain that the shape of the ε_f peak strongly depends on the dispersion of the corresponding transition-metal *4d* bands. On the other hand, the spectral function in the low-energy scale allows us to observe the development of the Kondo resonance and its satellites as the temperature is reduced. However, this technique predicts that the Kondo temperatures (T_K) are below 1 K, which is incorrect. Even if within this approach the Kondo resonance is not completely developed, an extrapolation out of the spectral function leads to $T_K(\mathrm{Rh})>T_K(\mathrm{Ru})>T_K(\mathrm{Pd})$ as in the experiments. However, one should be cautious even about the trend of the Kondo temperatures since the method has numerical instabilities at low temperatures and cannot, therefore, produce accurate Kondo temperatures at very low temperatures. The infinite value of the Coulomb interaction might also be a problem and calculations using finite values of U, like the DMFT, are highly desirable.[22]

It is surprising that the Kondo temperature of $CeRh_2Si_2$ is the highest among the series despite the assumption that the value of T_K is dictated by the strength of the hybridization at the Fermi level. This assumption seems not to always hold, as it was shown to break down for a cubic system of $CePd_3$.[1] This assumption is appropriate for systems in which the conduction band is mainly formed by highly delocalized *s* and/or *p* electrons. But if the main contribution to the conduction band is of *4d* character, as is the case in the tetragonal compounds studied here and for $CePd_3$, detailed hybridization calculations become crucial to describe properly the electronic properties.

Taking into account that $CeRh_2Si_2$ is a peculiar system presenting anomalous behaviors in several properties as compared to other members of the CeM_2Si_2 class of materials, it is not surprising that the crystal-field splittings of the $4f$ state or the value of T_K in $CeRh_2Si_2$ are greater than in $CePd_2Si_2$ and $CeRu_2Si_2$. The many-body NCA approach, used here, can pick up these features just because the hybridization function is calculated from first principles and thereafter contains detailed information of the electronic structure.

AKNOWLEDGMENTS

We would like to acknowledge helpful discussion with Jong Han regarding the implementation of the NCA method. This work was partially funded by UBACyT-X115 and the French-Argentinian collaboration program ECOS-SETCIP A00E04. A.M.L. belongs to *Consejo Nacional de Investigaciones Científicas y Técnicas*, Argentina (CONICET).

[1] J. E. Han, M. Alouani, and D. L. Cox, Phys. Rev. Lett. **78**, 939 (1997).
[2] N. Kioussis, B. R. Cooper, and J. M. Wills, Phys. Rev. B **44**, 10 003 (1991).
[3] J. M. Wills and B. R. Cooper, Phys. Rev. B **36**, 3809 (1987).
[4] R. Monnier, L. Degiorgi, and D. D. Koelling, Phys. Rev. Lett. **56**, 2744 (1986).
[5] F. Steglich, C. Geibel, S. Horn, U. Ahlheim, M. Lang, G. Sparn, A. Loidl, A. Krimmel, and W. Assmus, J. Magn. Magn. Mater. **90-91**, 383 (1990).
[6] L. C. Gupta, D. E. Mac Laughlin, Cheng Tien, C. Godart, M. A. Edwards, and R. D. Parks, Phys. Rev. B **28**, 3673 (1983).
[7] M. J. Besnus, J. P. Kappler, P. Lehmann, and A. Mesher, Solid State Commun. **55**, 779 (1985).
[8] R. A. Steeman, E. Frikkee, R. B. Helmholdt, A. A. Menovsky, J. van den Berg, G. J. Nieuwenhuys, and J. A.- Mydosh, Solid State Commun. **66**, 103 (1988).
[9] B. H. Grier, J. M. Lawrence, V. Murgai, and R. D. Parks, Phys. Rev. B **29**, 2664 (1984).
[10] S. Quezel, J. Rossat-Mignot, B. Chevalier, P. Lejay, and J. Etorneau, Solid State Commun. **49**, 685 (1984).
[11] S. Araki, R. Settai, T. C. Kabayashi, H. Harima, and Y. Önuki, Phys. Rev. B **64**, 224417 (2001).
[12] Shuzo Kawarazaki, M. Sato, Y. Miyako, N. Chigusa, K. Watanabe, N. Metoki, Y. Koike, and M. Nishi, Phys. Rev. B **61**, 4167 (2000).
[13] V. Vildosola, A. M. Llois, and J. G. Sereni, Phys. Rev. B **69**, 125116 (2004).
[14] T. Takeuchi *et al.*, Phys. Rev. B **67**, 064403 (2003).
[15] A. Severing, E. Holland-Moritz, B. D. Rainford, S. R. Culverhouse, and B. Frick, Phys. Rev. B **39**, 2557 (1989).
[16] P. Blaha, K. Schwarz, G. Madsen, D. Kvasnicka, and J. Luitz, *An Augmented Plane Wave + Local Orbitals Program for Calculating Crystal Properties* (Karlheinz Schwarz, Techn. Universitat Wien, Austria, 1999).
[17] O. Gunnarsson, O. K. Andersen, O. Jepsen, and J. Zaanen, Phys. Rev. B **39**, 1708 (1989).
[18] K. R. Lea, M. J. Leask, and W. P. Wolf, J. Phys. Chem. Solids **23**, 1381 (1962).
[19] N. E. Bickers, Rev. Mod. Phys. **59**, 845 (1987).
[20] N. E. Bickers, D. L. Cox, and J. W. Wilkins, Phys. Rev. B **36**, 2036 (1987).
[21] O. Gunnarsson and K. Schönhammer, Phys. Rev. Lett. **50**, 604 (1983).
[22] A. Georges, G. Kotliar, W. Krauth, and M. Rosenberg, Rev. Mod. Phys. **68**, 13 (1996).
[23] S. Imada *et al.*, J. Magn. Magn. Mater. **177-181**, 387 (1998).
[24] M. Tsunekawa *et al.*, Solid State Commun. **103**, 659 (1997).
[25] R. D. Parks, B. Reihl, N. Martensson, and F. Steglich, Phys. Rev. B **27**, 6052 (1983).
[26] J. P. Perdew and Y. Wang, Phys. Rev. B **45**, 13 244 (1992).
[27] H. Abe, H. Kitasawa, H. Suzuki, G. Kido, and T. Matsumoto, J.

Magn. Magn. Mater. **177-181**, 479 (1998).
[28] N. H. van Dijk, B. Fåk, T. Charvolin, P. Lejay, and J. M. Mignot, Phys. Rev. B **61**, 8922 (2000).
[29] R. Settai, A. Misawa, S. Araki, M. Kosaki, K. Sugiyama, T. Takeuchi, K. Kindo, Y. Haga, E. Yamamoto, and Y. Onuki, J. Phys. Soc. Jpn. **66**, 2260 (1997).
[30] M. J. Besnus, J. P. Kappler, P. Lehmann, and A. Mesher, Solid State Commun. **55**, 779 (1985).
[31] G. Zwicknagl, Adv. Phys. **41**, 203 (1992).
[32] R. J. Birgeneau, E. Bucher, J. P. Maitaand L. Passell, and K. C. Turberfield, Phys. Rev. B **8**, 5345 (1973).